Mechanisms of ethylene epoxidation over silver from machine-learning accelerated first-principles modeling and micro-kinetic simulations

Jin-Xun Liu[1,2], Shawn Lu[1], Shiuan-Bai Ann[1] and Suljo Linic[1]*

[1]Department of Chemical Engineering, University of Michigan – Ann Arbor, Ann Arbor, Michigan, 48109, USA

[2]Department of Chemical Physics, School of Chemistry and Materials Science, University of Science and Technology of China, Hefei, Anhui 230026, China

E-mail: linic@umich.edu

Abstract

We employed machine learning-augmented Density Functional Theory (DFT) thermodynamic calculations to assess the stability of different AgO_x structures under catalytic ethylene epoxidation reaction conditions. We found that there are multiple AgO_x surface motifs that could co-exist under the relevant conditions. These included Ag surface oxides (e.g. AgO_p(4x4) and $Ag_{1.83}O$) and atomic oxygen-covered Ag(111) surfaces. Furthermore, we employed DFT calculations to evaluate the energetics of different reaction mechanisms by which ethylene and oxygen can react on these surfaces. These studies revealed several energetically viable reaction pathways for ethylene epoxidation. Microkinetic modeling analyses, based on the DFT-calculated reaction pathways, showed that ethylene epoxidation can proceed on all surfaces and that multiple pathways, including those involving Langmuir-Hinshelwood and Eley-Rideal mechanisms, could be involved in selective and unselective reactions. The diversity of mechanisms that we discovered in the context of the relatively simple ethylene epoxidation reaction on Ag suggests that the richness and complexity of surface chemistry is most likely a rule rather than an exception in heterogeneous catalytic chemical transformations on metal surfaces, and that the concept of a single or even a dominant mechanism and reaction intermediates might need to be revisited for many reactions.

Keywords: Ethylene epoxidation on Ag, Epoxidation mechanisms, Artificial neural network potential, Grand canonical Monte Carlo, Microkinetic modeling

Introduction

Ethylene oxide (EO) is an important gateway chemical widely employed in the manufacturing of ethylene glycol, textiles, detergents, and many other chemical products.[1,2] EO is currently produced *via* the partial oxidation of ethylene, with CO_2 as a major nonselective byproduct.[3] Selectivity to EO is the main figure of merit in the process[4–11] with solid silver (Ag) nanoparticle catalysts being the only monometallic material achieving reasonably high EO selectivity.[9,12–14] Fundamental reasons for the uniqueness of Ag and the corresponding molecular mechanisms that can explain the process selectivity on Ag have been vigorously debated since the process discovery.[11,15–24] Specifically, there are questions about the active phase of Ag (oxide versus metal), the nature of selective oxygen species on the surface of Ag catalysts under reaction conditions, and the molecular mechanism by which oxygen and ethylene combine to form EO on the catalyst surface.[25–40]

In this work, we use machine learning accelerated first-principles calculations to study the active species of oxygen and the ethylene epoxidation mechanism on Ag model surfaces. Specifically, the compositions and structures of the Ag(111) surface over a wide range of temperatures and oxygen partial pressures were determined using grand canonical Monte-Carlo (GCMC) and *ab initio* thermodynamic simulations. Artificial Behler-Parrinello[41] neural network potential (ANNP) energy calculations were used to approximate the ground-state energy of DFT calculations for many possible AgO_x configurations. The inputs of these simulations were used in GCMC and *ab initio* thermodynamic modeling to establish a phase diagram[26,27,42,43] for AgO_x surfaces under realistic ethylene epoxidation conditions. Furthermore, DFT calculations were performed to study different ethylene epoxidation mechanisms on the most thermodynamically stable AgO_x surface configurations. These studies revealed that on the majority of likely thermodynamically stable AgO_x surfaces, ethylene epoxidation proceeds through the Langmuir-Hinshelwood (LH) mechanism involving an oxametallacycle (OMC) intermediate[20,29,34,44]. We also find that on the AgO_*p*(4×4) surface, the Eley–Rideal (ER) mechanism is dominant with ethylene molecules directly interacting with surface oxygen atoms. Our studies point towards the existence of multiple active AgO_x surface phases as well as multiple molecular mechanisms that can be activated under realistic ethylene epoxidation reaction conditions. The variety of mechanisms that we discovered in the context of the relatively simple ethylene epoxidation reaction suggests that the richness

and complexity of surface chemistry is most likely a rule rather than an exception in catalytic chemical transformations on metal surfaces and that the concept of a single or even a dominant mechanism and reaction intermediates, might need to be revisited for many reactions.

Results and Discussions

The surface compositions and structures of a functioning catalyst are highly dependent on the reaction conditions, namely, the temperature and partial pressures of reactants. For example, it has been suggested based on multiple experimental studies[45,46] that the Ag catalyst is either oxidized or metallic under epoxidation conditions. Additionally, in general, there is no agreement on the geometric structure of the oxidized Ag surface under reaction conditions. To address this question, we employed GCMC simulations accelerated by artificial neural network potential (ANNP) energy calculations (**Figure S1 – S4** and **Table S1 – S2**) to evaluate the thermodynamic stability of the Ag(111) surface in contact with gas phase O_2. The chemical potential of gas phase O_2 was considered for conditions ranging from 100 K to 600 K at a constant O_2 pressure of 1 atm, and for gas phase O_2 pressures ranging from 10^{-10} atm to 10^{8} atm at a constant temperature of 500 K. In addition to using the GCMC-ANNP framework to evaluate the stability of various AgO_x configurations with O atoms on the surface or sub-surface, we also used the *ab initio* thermodynamic approach to evaluate the stability of a few Ag-oxide phases, mainly $Ag_2O(111)$, $Ag_{1.83}O(111)$ and AgO_*p*(4×4) surfaces[47–49] that have been experimentally observed on well-defined Ag model surface in surface science experiments.

The data in **Figure 1a** show the calculated free surface energies normalized to the surface area for various AgO_x phases as a function of the O_2 chemical potential. Stars and dots represent the most stable phases computed using the GCMC-ANNP framework as a function of the O_2 pressure and temperature over the *p*(3×3) supercell (*i.e.*, we considered the AgO_1/9ML, 2/9ML, and 11/9ML structures). The lines describe the free energies computed for specific structures, shown in **Figure 1b-e** and **Figure S5**, as a function of external conditions using the *ab initio* thermodynamics framework. The oxygen surface coverages are reported as the ratio between the numbers of adsorbed oxygen atoms and surface Ag atoms.

The GCMC-ANNP data show that the Ag(111) surface is clean (no O adsorbate on the surface) over a wide range of conditions corresponding to relatively low chemical

potential of gas phase oxygen. The stable configurations among the configurations that contain only on-surface oxygen atoms on Ag(111) (no in-surface or sub-surface) are those with 1/9, 2/9 and 11/9 ML coverage (at very high O_2 chemical potentials corresponding to low temperature and/or high oxygen pressure). We note that further lowering the surface oxygen coverage to 1/16 ML can increase the stability of the Ag(111) surface under an oxygen atmosphere due to the reduction in the repulsive lateral interactions among the oxygen adsorbates. Therefore, we also analyzed the behavior of this surface structure. It is interesting to note that these on-surface oxygen structures are not thermodynamically stable compared to the surface oxide structures where oxygen atoms are either embedded in the surface Ag layer or positioned subsurface with respect to the surface Ag(111) layer, at any conditions that result in more than 1/16 ML O coverage. At these higher coverages, the repulsive electrostatic O-O on-surface interactions start pushing O atoms sub-surface.

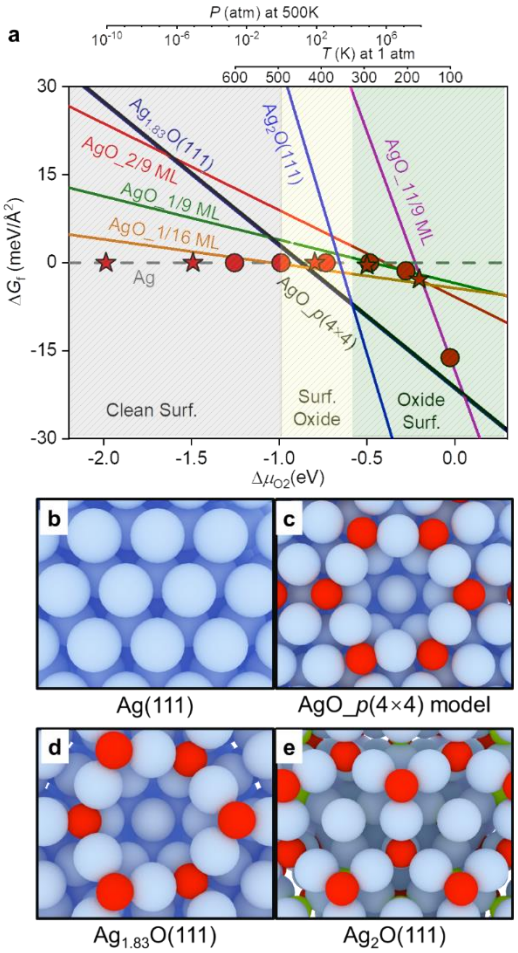

Figure 1. (**a**) Phase diagram of AgO_x structures in equilibrium with gas phase O_2. Gibbs surface free energies for AgO_x structures with *p*(3×3) supercells (*i.e.* AgO_1/9ML, 2/9ML,

and 11/9ML) identified by the GCMC-ANNP simulations at different temperatures (fixed pressure) and different O_2 partial pressures (fixed temperature) are denoted by solid dots and stars, respectively. The labels x in AgO_xML indicate oxygen concentrations on Ag(111) surfaces. The Gibbs surface free energies of the Ag_2O(111), $Ag_{1.83}O$(111) and AgO_*p*(4×4) surfaces relative to the Ag(111) surface are also shown. All the Gibbs formation energies of AgO_x surfaces were calculated with respect to the Ag(111) surface and O_2 molecules in the gas phase, which is reference state of zero free energy. We note that, despite having different stoichiometries and surface configurations of Ag and O, the $Ag_{1.83}O$(111) and AgO_p(4x4) overlap due to their similar Gibbs formation energies (3.10 meV/Å^2 vs 2.65 meV/Å^2 at 500 K) and the same oxygen concentration. (**b** – **e**) Representative Ag(111) surfaces under oxidation reaction conditions. There are abundant Ag vacancies on $Ag_{1.83}O$(111) surface, which is different from the stoichiometric Ag_2O(111) surface. The blue, red and green spheres are Ag atoms, surface oxygen atoms, and subsurface oxygen atoms within the 2nd Ag layer, respectively. The dark red spheres are subsurface oxygen atoms within or beyond the 3rd Ag layer.

It is important to realize that ethylene epoxidation under steady state conditions does not necessarily take place on the most thermodynamically stable AgO_x structures where the equilibrium between gas phase oxygen and the adsorbed oxygen can be assumed, *i.e.*, due to the presence of ethylene and due to potential kinetic limitations in activating O_2, the oxygen coverage might be lower than the equilibrium coverage. Therefore, it is reasonable to assume that the functioning Ag surfaces are likely to be a mixture of the equilibrium, $Ag_{1.83}O$(111), AgO_*p*(4×4), AgO_1/16ML surface oxide structures, as well as reduced quasi-stable structures such as AgO_1/9ML, which while not being the most stable surface configurations under conditions, still have relatively low Gibbs free formation energies.

Guided by the analysis above, we studied the ethylene epoxidation mechanisms on these stable and quasi-stable AgO_x surfaces, assuming that both molecular and atomic oxygen can serve as the source of oxygen atoms in the reaction coordinates (**Table S3 – S6, Figure 2** and **Figure S6 – S7a-f**). We focused on multiple chemical pathways, including ethylene epoxidation proceeding *via* LH and ER mechanisms. We established that the lowest energy LH pathway on all surfaces involves the dissociation of O_2 followed by adsorbed ethylene reacting with the dissociated atomic oxygen to form an oxametallacycle (OMC) intermediate, which is further isomerized into EO or acetaldehyde

(AA) products to complete the catalytic cycle. We note that further combustion of AA on AgO_x surfaces leads to the CO_2 byproduct.[22] The ease of AA combustion on Ag surfaces is well established[50–53] and therefore, we did not study it in this work. Alternatively, gas-phase ethylene can react with dissociated atomic oxygen species, forming EO directly *via* an ER mechanism.

The optimized transition state configurations and corresponding Gibbs free energy diagrams of ethylene epoxidation following the above-described LH and ER mechanisms over various AgO_x surfaces are shown in **Figure S8 – S12** and **Figure 2b – 2f** respectively. We also considered the mechanisms by which molecular O_2 is the oxidizing species (**Figure S7)**. In this mechanism, adsorbed ethylene first associates with the adsorbed molecular O_2, forming the $C_2H_4O_2$ intermediate, which is followed by OMC generation and transformation into EO and AA products following an LH mechanism. In addition to the LH mechanism, we also considered the direct oxidation of gaseous ethylene through its reaction with the adsorbed molecular O_2 via the ER mechanism (**Figure S7b - f**).

There are a few observations we can make based on a visual inspection of the computed reaction pathways in **Figures 2b – 2f** and **Figure S7**. Data show that ethylene epoxidation proceeding via the $C_2H_4O_2$ intermediate, except over AgO_2/9 ML surface, has a higher apparent activation barrier by at least 0.45 eV compared to the alternative mechanisms that involve atomic oxygen species in the generation of EO (**Figure S7g - S7k**). This is mainly due to the weak adsorption of both ethylene and O_2 molecules on different surfaces, which increases the Gibbs free energy of the systems (**Figure S7**). We also observe that the free energies of the intermediates on the AgO_2/9 ML surface are significantly higher than the free energies of the alternative surface structures, which makes this surface and the chemical pathways on this surface highly improbable. The Gibbs free energy diagrams in **Figure 2** also reveal that epoxidation proceeding with atomic oxygen *via* LH mechanism has a lower overall activation barrier than for the ER mechanism over all AgO_x surfaces, except for the AgO_*p*(4×4) surface, where the ER mechanism appears more energetically feasible. On the most stable metallic Ag surface (the AgO_1/16 ML surface) (**Figure 2b**), the isomerization of OMC into EO and AA has similar activation barriers with a difference of less than 0.02 eV, suggesting that both the selective and nonselective pathways are quite feasible and comparable. We also observe that the more oxidized $Ag_{1.83}O$ surface (**Figure 2e**), compared to more reduced AgO_x (i.e., the AgO_1/16 ML surface), has a lower barrier for the selective isomerization of OMC into

EO compared to the nonselective formation of AA, indicating that more oxygen-rich surfaces might be beneficial for EO product selectivity.

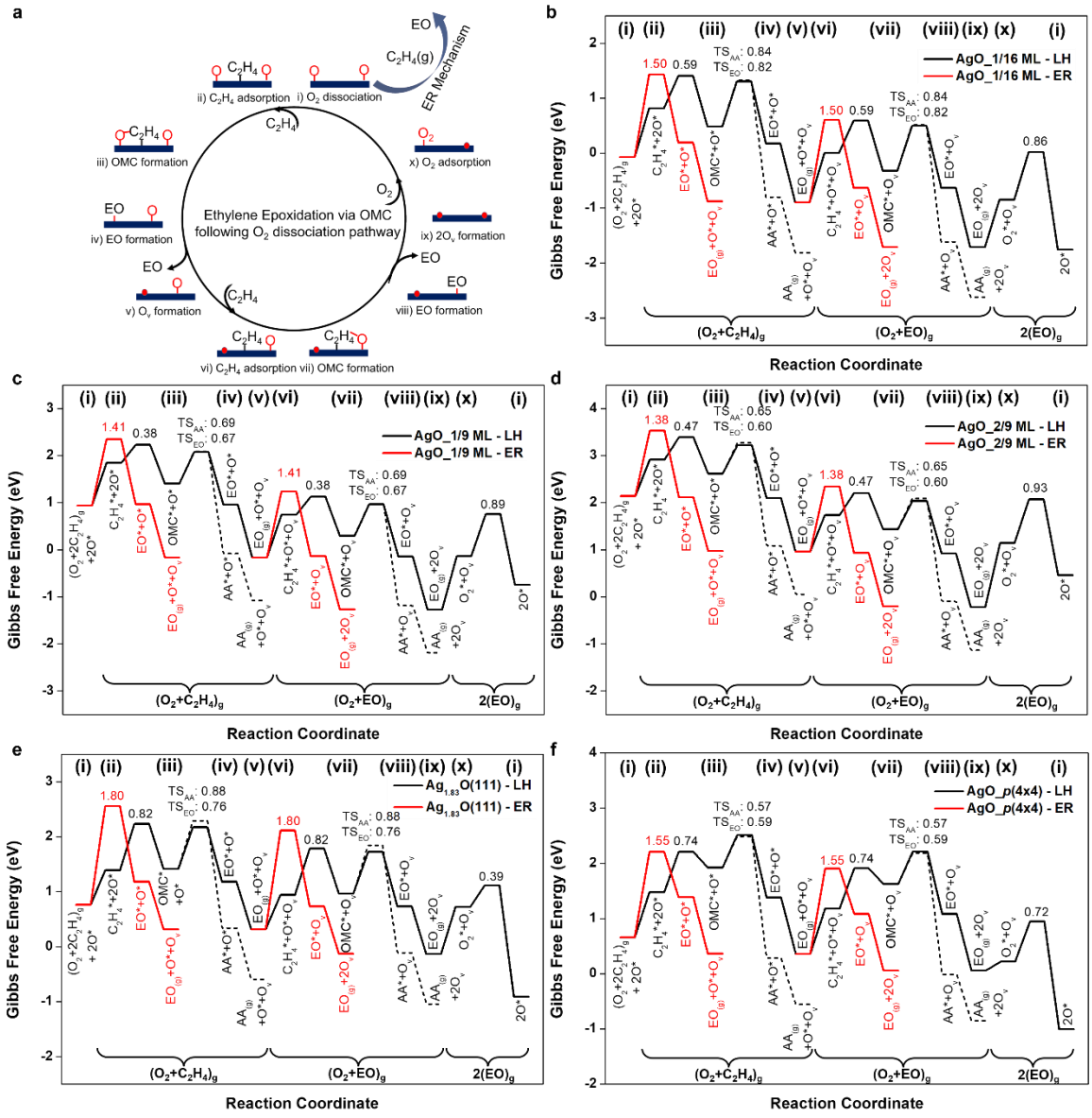

Figure 2. Ethylene oxidation mechanisms. (**a**) Scheme of elementary steps for ethylene epoxidation mechanism via atomic O* over Ag catalysts. In short, ethylene adsorbs on an atomic O*-covered Ag surface and reacts with atomic O* to form EO/AA. Molecular O_2 then dissociates on the Ag surface to replace the consumed O*. The scheme also considers the direct reaction of C_2H_4 in the gas phase with surface O*. O_v represents for

oxygen vacancy formed by the generation of EO and/or AA products. (**b** – **f**) Gibbs free energy diagrams of ethylene epoxidation over the AgO_xML (x = 1/16, 1/9 and 2/9), $Ag_{1.83}O$(111) and AgO_*p*(4×4) surfaces via (red line) ER mechanism and (black line) LH mechanism under typical ethylene oxidation conditions (T = 500 K and P_{O2} = P_{C2H4} = 1 atm), respectively. * indicates the active sites over AgO_x surfaces and Roman numeral labels in the energy diagrams correspond to the respective surface state listed in **Figure 2a**. The elementary activation barriers are shown in eV. The dashed lines indicate AA production by OMC transformation. The Gibbs free energies of all clean AgO_x surfaces, which is referred to Ag(111) surface and O_2 molecules in the gas phase, were normalized to *p*(3×3) unit cells for comparison. The bracket at the bottom of the figures show gas species also present in the system at the corresponding elementary steps.

To gain additional insight into the nature of molecular mechanisms in ethylene epoxidation, we also performed microkinetic simulations using the DFT-calculated energetics as input. The microkinetic simulation data were used to calculate the relative importance of different molecular mechanisms in ethylene epoxidation. The data is shown in **Figure 3** and **Figure S13** in the form of normalized reaction fluxes associated with different chemical pathways with which ethylene and oxygen can react on the different Ag surfaces. The data show that on the AgO_xML (x = 1/16 and 1/9) and $Ag_{1.83}O$ surfaces, ethylene epoxidation preferentially proceeds via a LH mechanism (**Figure 3a – 3c**), with a smaller fraction of molecules moving from the reactant to the product state via the ER mechanism. We also used microkinetic modeling to compute the degree of rate control (DRC) for each elementary step. The DRC is a measure of the kinetic relevance of a particular elementary step, *i.e.*, it allows us to investigate whether a particular elementary step is rate controlling or is kinetically irrelevant.[54–56] The data in **Figure 3e – 3f** indicate that on the AgO_xML (x = 1/16 and 1/9) surfaces, the reaction rate is controlled by the dissociation of O_2 resulting in a low surface coverage of atomic oxygen (**Figure S14**), while the EO selectivity is controlled by activation energy of the branching reactions of the OMC to EO and AA under ethylene epoxidation conditions (**Figure 2b - 2c**) (T = 500 K and P_{O2} = 1 bar).

The microkinetic simulation data also show that on the $Ag_{1.83}O$(111) surface, ethylene epoxidation proceeds through the LH mechanism with EO selectivity of over 90% (**Figure 3c**). This high selectivity is due to the lower activation barrier for the isomerization of OMC to EO than to AA over this surface (**Figure 2e**). The microkinetic analysis also

shows that adsorbed ethylene reacting with dissociated oxygen species in the formation of the OMC intermediate acts as the rate-determining step (RDS) for ethylene epoxidation on the $Ag_{1.83}O(111)$ surface (**Figure 3g**). On the other hand, we find that on the AgO_*p*(4×4) surface, the reaction preferentially proceeds via the ER mechanism and achieves the highest EO selectivity (**Figure 3d**). This preference for the ER mechanism on this surface can be attributed the stronger adsorption and higher surface coverage of atomic oxygen (**Figure S14**) in AgO_*p*(4×4) surface compared to the other surfaces, resulting in a more endothermic OMC intermediate formation and subsequent reaction through the LH mechanism (**Figure 2f**). We find that on this surface, gas-phase ethylene reacting directly with surface atomic oxygen via the ER mechanism is the rate-limiting step (**Figure 3h**).

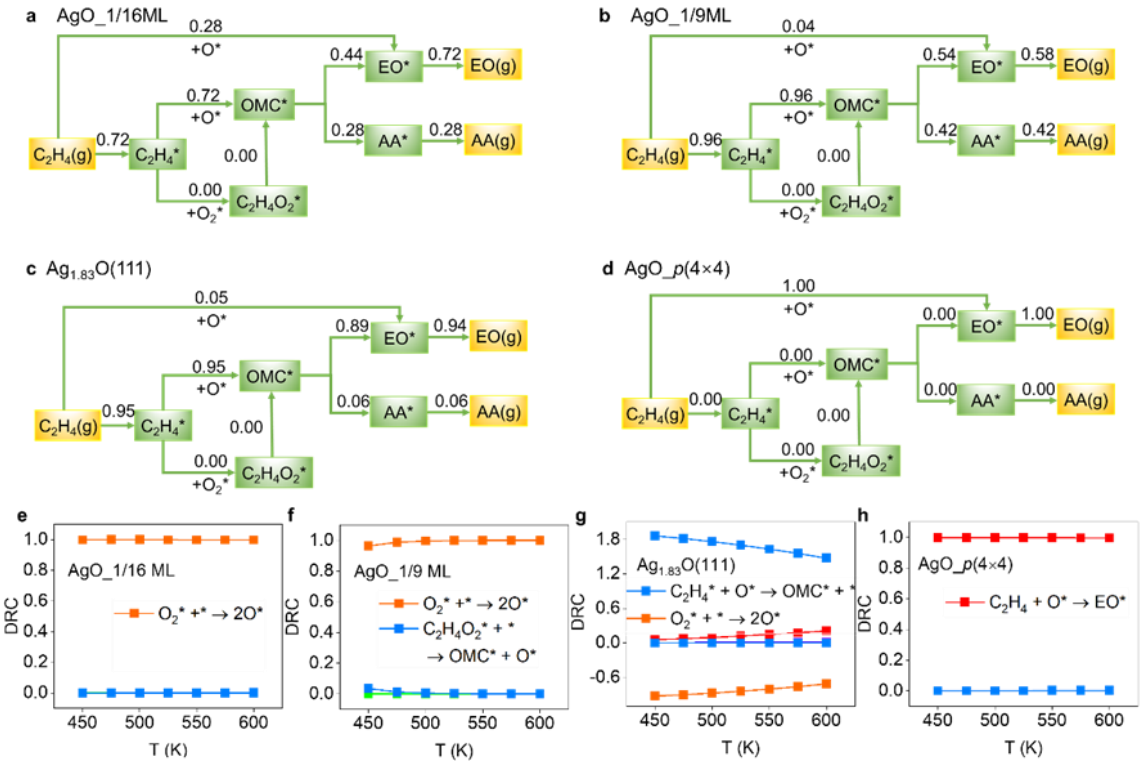

Figure 3. Reaction flux (**a** – **d**) and DRC (**e** – **h**) analyses for ethylene epoxidation over the AgO_1/16 ML, AgO_1/9 ML, $Ag_{1.83}O(111)$ and AgO_*p*(4×4) surfaces at 500 K determined by microkinetic simulations. The partial pressures of gas phase O_2 and ethylene are 1 atm. Different colors indicate distinct elementary steps and only reactions with an absolute DRC value greater than 0.05 are indicated for ethylene epoxidation via the mechanism shown in **Table S5 – S7** and **Figure S6 – S7**.

The microkinetic analysis of the feasible reaction pathways on Ag surfaces with different coverages of O atoms suggests that within the mechanisms discussed herein, higher O coverages might be beneficial for selectivity towards EO. For example, the data show that the highest EO selectivity is achieved on the $Ag_{1.83}O(111)$ and AgO_*p*(4×4) structures. Since the EO selectivity is mainly governed by the activation barrier difference between EO and AA formation via the isomerization of the OMC intermediate, in **Figure 4a** we show the calculated activation barriers for the two isomerization reactions on different AgO_x surfaces (active site motifs). The data in **Figure 4a** show that the isomerization of the OMC intermediate into EO and AA products on different AgO_x surfaces generally obeys the Brønsted-Evans-Polanyi (BEP) relationship[57,58] with very similar slopes. We note that the slope relates the heat of reaction to the activation barrier via the expressions in **Figure 4a**. This means that for the isomerization reactions, a more exothermic reaction will have a lower activation barrier. Since the BEP slopes for the OMC isomerization into AA and EO on different AgO_x surfaces are identical, the difference in the activation barriers on different surfaces can be attributed to the stronger adsorption of EO than AA on more oxidized AgO_x surfaces (**Table S3 – S4**).

Since significant discussion related to the mechanism of ethylene epoxidation on Ag is centered on the relationship between the electronic structure of reactive surface oxygen atoms and the product selectivity, we also investigated the difference in the electronic structure of different oxygen species by computing the Bader charge of oxygen on different AgO_x surfaces. The calculations showed that highly selective atomic oxygen on the AgO_*p*(4×4) surface has the largest Bader charge (Q_O = -0.98 |*e*|) (**Figure 4b**). This high Bader charge is consistent with the formation of the relatively strong Ag-O bonds. The charge transfer from surface Ag atoms to in-surface atomic oxygen proceeds through a hybridization of the in-plane O-*p* orbitals with the Ag-*d* band (**Figure 4c**). In contrast, the charge transfer between atomic oxygen and surface Ag atoms becomes smaller over the $Ag_{1.83}O(111)$ surface (Q_O = -0.95 |*e*|), which correlates with decreasing selectivity toward EO. Even less charge transfer between surface atomic oxygen species and Ag atoms (Q_O = -0.92 and -0.90 |*e*|) are computed over the AgO_1/16ML and AgO_1/9ML surfaces correlating with the lowest selectivity toward EO. The different Bader charge state of atomic oxygen over AgO_*p*(4×4), $Ag_{1.83}O(111)$ and AgO_x ML (x = 1/16 and 1/9) can be attributed to their different adsorption sites and surface motifs. Atomic oxygen prefers to adsorb in the fourfold site over AgO_*p*(4×4) surface and in the threefold site over the $Ag_{1.83}O(111)$ and AgO_x ML surfaces.

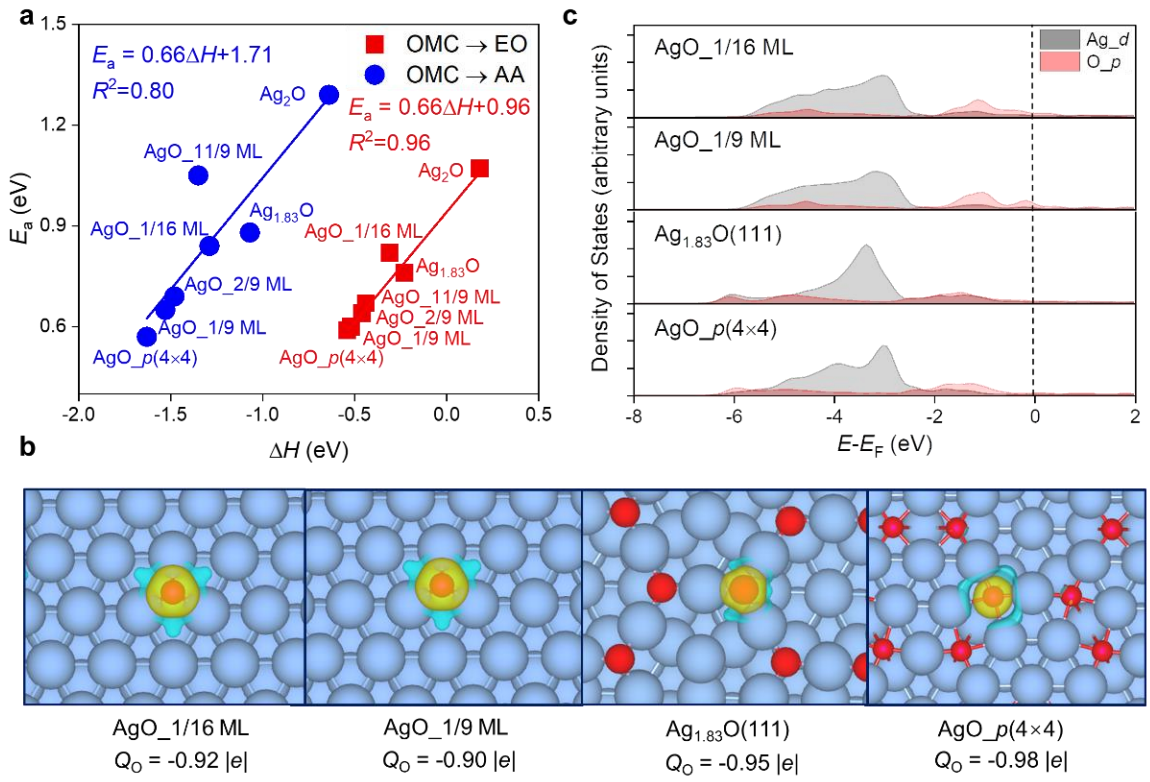

Figure 4. (**a**) Brønsted-Evans-Polanyi (BEP) relationships for the isomerization of OMC into EO and AA products. E_a and ΔH are the activation barrier and elementary reaction energies, respectively, for the isomerization of OMC to AA and EO. (**b**) Bader charge analysis and isosurfaces of differential charge density of surface atomic oxygen on AgO_x surfaces. The isovalue is set to 0.002 |e|/Å^3. Yellow and cyan colors represent charge depletion and accumulation, respectively. (**c**) Density of states (DOS) for atomic oxygen atoms on different AgO_x surfaces. Red and gray areas show the *p*-band of O and *d*-band of Ag atoms, respectively. The dashed line indicates the Fermi level.

Conclusions

We employed machine learning-augmented Density Functional Theory (DFT) thermodynamic calculations to show that there are multiple Ag-O_x surface motifs that could co-exist under ethylene epoxidation conditions. Microkinetic modeling analyses, based on the DFT-calculated reaction pathways on the thermodynamically accessible surfaces, showed that ethylene epoxidation can proceed on all surfaces and that multiple pathways, including those involving Langmuir-Hinshelwood and Eley-Rideal mechanisms, could be

involved in selective and unselective reactions. The diversity of molecular mechanisms that we discovered in the context of the relatively simple ethylene epoxidation reaction on Ag suggests that the richness and complexity of surface chemistry is most likely a rule rather than an exception in heterogeneous catalytic chemical transformations on metal surfaces, and that the concept of a single or even a dominant mechanism and reaction intermediates might need to be revisited for many reactions.

Methods

All the experimental and theoretical methodologies are presented in SI.

Data availability

The data that support the plots within this paper and other findings of this study are available from the corresponding authors upon reasonable request.

Acknowledgments

This work was supported through a grant from the Department of Energy Office of Basic Energy Sciences (DE-SC0021008). S. Lu acknowledges the support of a fellowship through the National Science Foundation Graduate Research Fellowship Program (NSF-GRFP).

Author contributions

S. Linic conceived the idea and supervised and directed the project. J.X. Liu performed the theoretical calculations and analyzed the DFT data. All authors discussed the results and wrote and commented on the paper.

Competing interests

The authors declare no competing interests.

Supplementary information

Supplementary information is available free of charge on the ACS Publications website.

- Computational methodologies (including DFT, Artificial Neural Network Potential (ANNP), Grand Canonical Monte Carlo (GCMC) and microkinetic simulations), tables of radial symmetry functions used to describe local atomic environments during ANNP training, tables of adsorption energies of various reactants, intermediates, and products for ethylene epoxidation over AgOx surfaces, table of forward and backward activation energies for ethylene epoxidation over AgOx surfaces, degree of rate control

calculations obtained through microkinetic simulations over AgOx surfaces, and table of detailed AgOx structure information.

References:

(1) *Toxicological Profile for Ethylene Oxide*; US Department of Health, Human Services: Atlanta, GA, 1990.
(2) *Evaluation of the Inhalation Carcinogenicity of Ethylene Oxide*; (Final Report):; U.S. Environmental Protection Agency: Washington, DC, EPA/635/R-16/350F, 2016.
(3) Satterfield, C. N. Heterogeneous Catalysis in Industrial Practice: McGraw–Hill, 1991.
(4) Torres, D.; Lopez, N.; Illas, F.; Lambert, R. M. Why Copper Is Intrinsically More Selective Than Silver in Alkene Epoxidation: Ethylene Oxidation on Cu (111) Versus Ag (111. *J Am Chem Soc* **2005**, *127*, 10774–10775.
(5) Rojluechai, S.; Chavadej, S.; Schwank, J. W.; Meeyoo, V. Catalytic Activity of Ethylene Oxidation over Au, Ag and Au–Ag Catalysts: Support Effect. *Catal Commun* **2007**, *8*, 57–64.
(6) Jiang, C.; Hara, K.; Fukuoka, A. Low-Temperature Oxidation of Ethylene over Platinum Nanoparticles Supported on Mesoporous Silica. *Angew Chem Int Ed* **2013**, *52*, 6265–6268.
(7) Greiner, M. T.; Jones, T. E.; Klyushin, A.; Knop-Gericke, A.; Schlögl, R. Ethylene Epoxidation at the Phase Transition of Copper Oxides. *J Am Chem Soc* **2017**, *139*, 11825–11832.
(8) Christopher, P.; Linic, S. Engineering Selectivity in Heterogeneous Catalysis: Ag Nanowires as Selective Ethylene Epoxidation Catalysts. *J Am Chem Soc* **2008**, *130*, 11264–11265.
(9) Li, H.; Cao, A.; Nørskov, J. K. Understanding Trends in Ethylene Epoxidation on Group Ib Metals. *ACS Catal* **2021**, *11*, 12052–12057.
(10) Xu, H.; Zhu, L.; Nan, Y.; Xie, Y.; Cheng, D. Revisit the Role of Metal Dopants in Enhancing the Selectivity of Ag-Catalyzed Ethylene Epoxidation: Optimizing Oxophilicity of Reaction Site Via Cocatalytic Mechanism. *ACS Catal* **2021**, *11*, 3371–3383.
(11) Christopher, P.; Linic, S. Overcoming Limitation in the Design of Selective Heterogeneous Catalysts by Manipulating Shape and Size of Catalytic Particles: Epoxidation Reactions on Silver. *ChemCatChem* **2010**, *2*, 1061.
(12) Averill, B.; Moulijn, J.; Santen, R.; Leeuwen, P. Catalysis: An Integrated Approach; Elsevier: Amsterdam. *The Netherlands* **1999**.
(13) Ozbek, M.; Onal, I.; Santen, R. Why Silver Is the Unique Catalyst for Ethylene Epoxidation. *J Catal* **2011**, *284*, 230–235.
(14) Greiner, M.; Jones, T.; Johnson, B.; Rocha, T.; Wang, Z.-J.; Armbrüster, M.; Willinger, M.; Knop-Gericke, A.; Schlögl, R. The Oxidation of Copper Catalysts During Ethylene Epoxidation. *Phys Chem Chem Phys* **2015**, *17*, 25073–25089.
(15) Christopher, P.; Linic, S. Shape- and Size-Specific Chemistry of Ag Nanostructures in Catalytic Ethylene Epoxidation. *ChemCatChem* **2010**, *2*, 78–83.
(16) Ozbek, M. O.; Onal, I.; van Santen, R. A. Ethylene Epoxidation Catalyzed by Silver Oxide. *ChemCatChem* **2011**, *3* (1), 150–153.
(17) Reijen, J. E.; Kanungo, S.; Welling, T. A. J.; Versluijs-Helder, M.; Nijhuis, T. A.; Jong, K. P.; Jongh, P. E. Preparation and Particle Size Effects of Ag/A-Al2o3 Catalysts for Ethylene Epoxidation. *J Catal* **2017**, *356*, 65–74.
(18) Huš, M.; Hellman, A. Dipole Effect on Ethylene Epoxidation: Influence of Alkali Metals and Chlorine. *J Catal* **2018**, *363*, 18–25.
(19) Jones, T. E.; Wyrwich, R.; Böcklein, S.; Carbonio, E. A.; Greiner, M. T.; Klyushin, A. Y.; Moritz, W.; Locatelli, A.; Menteş, T. O.; Niño, M. A.; Knop-Gericke, A.; Schlögl, R.;

Günther, S.; Wintterlin, J.; Piccinin, S. The Selective Species in Ethylene Epoxidation on Silver. *ACS Catal* **2018**, *8*, 3844–3852.
(20) Linic, S.; Barteau, M. A. Control of Ethylene Epoxidation Selectivity by Surface Oxametallacycle. *J Am Chem Soc* **2003**, *125*, 4034.
(21) Carbonio, E. A.; Rocha, T. C. R.; Klyushin, A. Y.; Pis, I.; Magnano, E.; Nappini, S.; Piccinin, S.; Knop-Gericke, A.; Schlogl, R.; Jones, T. E. Are Multiple Oxygen Species Selective in Ethylene Epoxidation on Silver? *Chem. Sci.* **2018**, *9*, 990–998.
(22) Reijen, J. E.; Versluis, W. C.; Kanungo, S.; d'Angelo, M. F.; Jong, K. P.; Jongh, P. E. From Qualitative to Quantitative Understanding of Support Effects on the Selectivity in Silver Catalyzed Ethylene Epoxidation. *Catal Today* **2019**, *338*, 31–39.
(23) Hoof, A.; Hermans, E.; Bavel, A.; Friedrich, H.; Hensen, E. J. Structure Sensitivity of Silver-Catalyzed Ethylene Epoxidation. *ACS Catal* **2019**, *9*, 9829–9839.
(24) Harris, J. W.; Herron, J. A.; DeWilde, J. F.; Bhan, A. Molecular Characteristics Governing Chlorine Deposition and Removal on Promoted Ag Catalysts During Ethylene Epoxidation. *J Catal* **2019**, *377*, 378–388.
(25) Carlisle, C.; King, D.; Bocquet, M.-L.; Cerdá, J.; Sautet, P. Imaging the Surface and the Interface Atoms of an Oxide Film on Ag 111 by Scanning Tunneling Microscopy: Experiment and Theory. *Phys Rev Lett* **2000**, *84*, 3899.
(26) Reuter, K.; Scheffler, M.; Composition. Structure, and Stability of Ruo2(110) as a Function of Oxygen Pressure. *Phys Rev B* **2001**, *65*, 035406.
(27) Li, W.-X.; Stampfl, C.; Scheffler, M. Why Is a Noble Metal Catalytically Active? The Role of the O-Ag Interaction in the Function of Silver as an Oxidation Catalyst. *Phys Rev Lett* **2003**, *90*, 256102.
(28) Bocquet, M.-L.; Michaelides, A.; Loffreda, D.; Sautet, P.; Alavi, A.; King, D. A. New Insights into Ethene Epoxidation on Two Oxidized Ag 111 Surfaces. *J Am Chem Soc* **2003**, *125*, 5620–5621.
(29) Linic, S.; Piao, H.; Adib, K.; Barteau, M. A. Ethylene Epoxidation on Ag: Identification of the Crucial Surface Intermediate by Experimental and Theoretical Investigation of Its Electronic Structure. *Angew Chem Int Ed* **2004**, *43*, 2918–2921.
(30) Stegelmann, C.; Schiodt, N. C.; Campbell, C. T.; Stoltze, P. Microkinetic Modeling of Ethylene Oxidation over Silver. *J. Catal.* **2004**, *221* (2), 630–649.
(31) Michaelides, A.; Reuter, K.; Scheffler, M. When Seeing Is Not Believing: Oxygen on Ag (111), a Simple Adsorption System? *J Vac Sci Technol A* **2005**, *23*, 1487–1497.
(32) Gao, W.; Zhao, M.; Jiang, Q. A Dft Study on Electronic Structures and Catalysis of Ag12o6/Ag (111) for Ethylene Epoxidation. *J Phys Chem C* **2007**, *111*, 4042–4046.
(33) Martin, N.; Klacar, S.; Gronbeck, H.; Knudsen, J.; Schnadt, J.; Blomberg, S.; Gustafson, J.; Lundgren, E. High-Coverage Oxygen-Induced Surface Structures on Ag (111. *J Phys Chem C* **2014**, *118*, 15324–15331.
(34) Linic, S.; Barteau, M. A. Formation of a Stable Surface Oxametallacycle That Produces Ethylene Oxide. *J. Am. Chem. Soc.* **2002**, *124* (2), 310–317.
(35) Özbek, M.; Santen, R. The Mechanism of Ethylene Epoxidation Catalysis. *Catal Lett* **2013**, *143*, 131–141.
(36) Chen, D.; Kang, P.-L.; Liu, Z.-P. Active Site of Catalytic Ethene Epoxidation: Machine-Learning Global Pathway Sampling Rules out the Metal Sites. *ACS Catal* **2021**, *11*, 8317–8326.
(37) Wu, S.; Tatarchuk, B. J.; Adamczyk, A. J. Ethylene Oxidation on Unpromoted Silver Catalysts: Reaction Pathway and Selectivity Analysis Using Dft Calculations. *Surf Sci* **2021**, *708*, 121834.
(38) Huš, M.; Hellman, A. Ethylene Epoxidation on Ag (100), Ag (110), and Ag (111): A Joint Ab Initio and Kinetic Monte Carlo Study and Comparison with Experiments. *ACS Catal* **2018**, *9*, 1183–1196.
(39) Hoof, A. J.; Filot, I. A.; Friedrich, H.; Hensen, E. J. Reversible Restructuring of Silver Particles During Ethylene Epoxidation. *ACS Catal* **2018**, *8*, 11794–11800.

(40) Pu, T.; Tian, H.; Ford, M. E.; Rangarajan, S.; Wachs, I. E. Overview of Selective Oxidation of Ethylene to Ethylene Oxide by Ag Catalysts. *ACS Catal.* **2019**, *9* (12), 10727–10750.
(41) Behler, J.; Parrinello, M. Generalized Neural-Network Representation of High-Dimensional Potential-Energy Surfaces. *Phys Rev Lett* **2007**, *98*, 146401.
(42) Rebsdat, S.; Mayer, D. Ethylene Oxide. *Ullmanns Encycl. Ind. Chem.* **2001**.
(43) Liu, J.-X.; Su, Y.; Filot, I. A.; Hensen, E. J. A Linear Scaling Relation for CO Oxidation on CeO2-Supported Pd. *J Am Chem Soc* **2018**, *140*, 4580–4587.
(44) Greeley, J.; Mavrikakis, M. On the Role of Subsurface Oxygen and Ethylenedioxy in Ethylene Epoxidation on Silver. *J. Chem. C* **2007**, *111* (22), 7992–7999.
(45) Santen, R.; Groot, C. The Mechanism of Ethylene Epoxidation. *J Catal* **1986**, *98*, 530–539.
(46) Bukhtiyarov, V. I.; Havecker, M.; Kaichev, V. V.; Knop-Gericke, A.; Mayer, R. W.; Schlogl, R. Atomic Oxygen Species on Silver: Photoelectron Spectroscopy and x-Ray Absorption Studies. *Phys. Rev. B* **2003**, *67*, 235422.
(47) Bocquet, M.-L.; Sautet, P.; Cerda, J.; Carlisle, C. I.; Webb, M. J.; King, D. A. Specific Ethene Surface Activation on Silver Oxide Covered Ag111 from the Interplay of Stm Experiment and Theory. *J Am Chem Soc* **2003**, *125*, 3119–3125.
(48) Schnalt J.; Michaelides A.; Knudsen J.; Vang R. T.; Reuter K.; Lægsgaard E.; Scheffler M.; Besenbacher F. *Phys Rev Lett* **2006**, *96*, 146101.
(49) Andryushechkin, B. V.; Shevlyuga, V. M.; Pavlova, T. V.; Zhidomirov, G. M.; Eltsov, K. N. Adsorption of O2 on Ag(111): Evidence of Local Oxide Formation. *Phys Rev Lett* **2016**, *117*, 056101.
(50) Mao, C.-F.; Vannice, M. A.; Iii, H. S. A. A.-A. Oxidation of Ethylene, Ethylene Oxide, and Acetaldehyde over Silver Dispersed on High Surface Area A-Alumina. *Appl Catal Gen* **1995**, *122*, 61–76.
(51) Epling, W. S.; Hoflund, G. B.; Minahan, D. M.; Cs-Promoted, S. A-Alumina-Supported Silver, Ethylene-Epoxidation Catalysts. *J Catal* **1997**, *171*, 490–497.
(52) Lukaski, A.; Barteau, M. A. Investigation of Ethylene Oxide on Clean and Oxygen-Covered Ag (110) Surfaces. *Catal Lett* **2009**, *128*, 9–17.
(53) Mukda, N.; Autthanit, C.; Praserthdam, P.; Jongsomjit, B. Production of Acetaldehyde Via Oxidative Dehydrogenation of Ethanol over AgLi/SiO2 Catalysts. *Bull Chem React Eng Catal* **2020**, 15.
(54) Campbell, C. T. Future Directions and Industrial Perspectives Micro-and Macro-Kinetics: Their Relationship in Heterogeneous Catalysis. *Top Catal* **1994**, *1*, 353–366.
(55) Campbell, C. T. Finding the Rate-Determining Step in a Mechanism: Comparing Dedonder Relations with the “Degree of Rate Control.” *J Catal* **2001**, *204*, 520–524.
(56) Stegelmann, C.; Andreasen, A.; Campbell, C. T. Degree of Rate Control: How Much the Energies of Intermediates and Transition States Control Rates. *J Am Chem Soc* **2009**, *131*, 8077–8082.
(57) Brønsted, J. Acid and Basic Catalysis. *Chem Rev* **1928**, *5*, 231–338.
(58) Evans, M.; Polanyi, M. Inertia and Driving Force of Chemical Reactions. *Trans. Faraday Soc.* **1938**, *34*, 11–24.

TOC

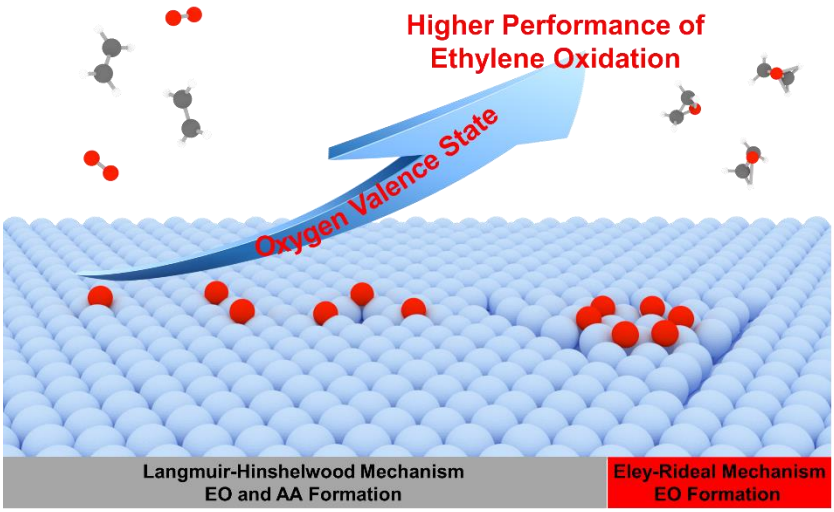
Higher Performance of
Ethylene Oxidation
Oxygen Valence State
Langmuir-Hinshelwood Mechanism
EO and AA Formation
Eley-Rideal Mechanism
EO Formation